# Multiwavelength observations of the black hole transient Swift J1745−26 during the outburst decay

E. Kalemci[1]⋆, M. Özbey Arabacı [2], T. Güver[3], D. M. Russell[4,5], J. A. Tomsick[6],
J. Wilms[7], G. Weidenspointner[8,9], E. Kuulkers[10], M. Falanga[11], T. Dinçer[1],
S. Drave[12], T. Belloni[13], M. Coriat[14], F. Lewis[15,16], T. Muñoz-Darias[17]

[1] *Faculty of Engineering and Natural Sciences, Sabancı University, Orhanlı-Tuzla, 34956, Istanbul, Turkey*

[2] *Physics Department, Middle East Technical University, 06530, Ankara, Turkey*

[3] *Astronomy and Space Sciences Department, Istanbul University, 34119, Universite, Istanbul, Turkey*

[4] *New York University Abu Dhabi, P.O. Box 129188, Abu Dhabi, United Arab Emirates*

[5] *Instituto de Astrofisica de Canarias, C/ Via Láctea, s/n E38205 - La Laguna (Tenerife), Spain*

[6] *Space Sciences Laboratory, 7 Gauss Way, University of California, Berkeley, CA, 94720-7450, USA*

[7] *Dr. Karl-Remeis-Sternwarte and Erlangen Centre for Astroparticle Physics, Friedrich Alexander Universität Erlangen-Nürnberg, Sternwartstr. 7, 96049 Bamberg, Germany*

[8] *European X-ray Free Electron Laser facility GmbH, Albert-Einstein-Ring 19, 22761, Hamburg, Germany*

[9] *Max Planck Institut für Extraterrestrische Physik, Garching, Germany*

[10] *European Space Agency, European Space Astronomy Centre, P.O. Box 78, 28691, Villanueva de la Canada, Madrid, Spain*

[11] *International Space Science Institute (ISSI), Hallerstrasse 6,CH-3012 Bern, Switzerland*

[12] *School of Physics and Astronomy, Faculty of Physical Sciences and Engineering, University of Southampton, University Road, Southampton, SO17 1BJ, UK*

[13] *INAF - Osservatorio Astronomico di Brera, Via E. Bianchi 46, I-23807, Merate, Italy*

[14] *Department of Astronomy, University of Cape Town, Private Bag X3, Rondebosch, 7701, South Africa*

[15] *Faulkes Telescope Project, University of South Wales, Pontypridd, CF37 1DL, Wales*

[16] *Astrophysics Research Institute, Liverpool John Moores University, IC2, Liverpool Science Park, 146 Brownlow Hill, Liverpool L3 5RF, UK*

[17] *University of Oxford, Department of Physics, Astrophysics, Keble Road, Oxford, OX1 3RH, United Kingdom*

submitted to mnras

**ABSTRACT**

We characterized the broad-band X-ray spectra of Swift J1745−26 during the decay of the 2013 outburst using *INTEGRAL* ISGRI, JEM-X and *Swift* XRT. The X-ray evolution is compared to the evolution in optical and radio. We fit the X-ray spectra with phenomenological and Comptonization models. We discuss possible scenarios for the physical origin of a ∼50 day flare observed both in optical and X-rays ∼170 days after the peak of the outburst. We conclude that it is a result of enhanced mass accretion in response to an earlier heating event. We characterized the evolution in the hard X-ray band and showed that for the joint ISGRI-XRT fits, the e-folding energy decreased from 350 keV to 130 keV, while the energy where the exponential cut-off starts increased from 75 keV to 112 keV as the decay progressed. We investigated the claim that high energy cut-offs disappear with the compact jet turning on during outburst decays, and showed that spectra taken with HEXTE on *RXTE* provide insufficient quality to characterize cut-offs during the decay for typical hard X-ray fluxes. Long *INTEGRAL* monitoring observations are required to understand the relation between the compact jet formation and hard X-ray behavior. We found that for the entire decay (including the flare), the X-ray spectra are consistent with thermal Comptonization, but a jet synchrotron origin cannot be ruled out.

**Key words:** X-rays: accretion, binaries - X-rays: binaries: close - Stars: individual: Swift J1745−26, Swift J174510.8−2624

## 1  INTRODUCTION

Galactic black hole transients (GBHT) are excellent laboratories to study the complex relation between the jet and
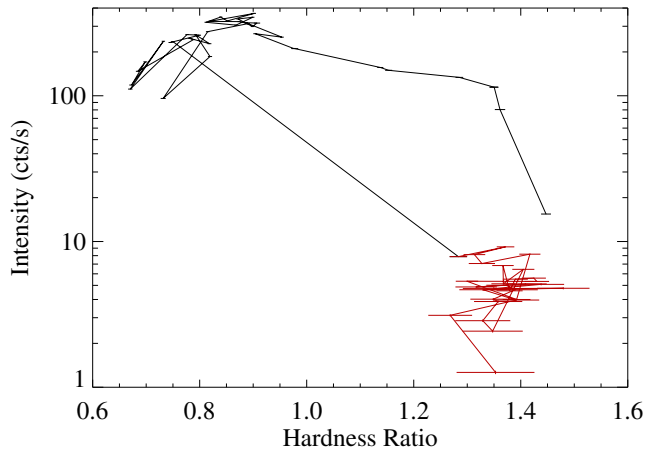
⋆ E-mail:ekalemci@sabanciuniv.edu

**Figure 1.** Hardness-Intensity diagram of Swift J1745−26 obtained using the *Swift* XRT data only. The hardness ratio is defined as ratio of counts in 2.5−10 keV and 1−2.5 keV bands and the intensity is the count rate in 1−10 keV band. Red data points represent the observations used in this work.

the accretion environment in X-ray binaries as the outbursts evolve on timescales of months, allowing detailed investigation of the properties of accretion states (traced by X-ray spectral and timing properties) together with the properties of jets traced by the radio, and optical/infrared (OIR) emission.

The evolution of accretion states throughout an outburst is best described by the hardness intensity diagram (HID, Homan et al. 2001; Belloni 2010). The HID of Swift J1745−26 is given in Figure 1. At the start of a typical outburst, the GBHT is in the hard state (HS), the lower right side of the HID. In this state, the X-ray spectrum is dominated by a hard, power-law like component, historically associated with Compton scattering of soft photons by a hot electron corona. Weak emission from a cool, optically thick, geometrically thin disk (modeled by a multi-temperature blackbody, Makishima et al. 1986) may also be observed. The variability is strong (typically >20% fractional rms amplitude). As the X-ray flux increases, the GBHT usually makes a transition to the soft state (upper-left side of the HID) in which the X-ray spectrum is dominated by the optically thick accretion disk. At the end of outbursts, sources go back to the hard state as the X-ray flux decreases. There are also intermediate states occurring during transitions between the soft and the hard states (see McClintock & Remillard 2006 and Belloni 2010 for details of spectral states of GBHTs).

In some cases, the evolution of spectral states during an outburst does not follow the usual pattern in the HID. The source can stay in the HS throughout the outburst or make a transition to a hard intermediate state while never fully entering the soft state. These are called "failed outbursts" (Brocksopp, Bandyopadhyay & Fender 2004; Soleri et al. 2013; Russell et al. 2013b). The HID of Swift J1745−26 given in Figure 1 is a typical HID for a failed outburst (see Capitanio et al. 2009; Ferrigno et al. 2012; Soleri et al. 2013, for other examples of failed outburst HIDs).

Contemporaneous multi-wavelength observations of GBHTs in optical, near infrared (OIR) and radio show that the behaviour of the jets are closely related to X-ray spectral states. Steady, compact jets are observed in the HS (Corbel et al. 2000; Fender 2001, 2010; Fender & Gallo 2014). The typical SEDs in the HS show a flat or inverted power-law at radio frequencies that breaks, at near- to mid-infrared wavelengths, to a second power-law with negative spectral index. Such an emission profile is consistent with emission from a compact, conical jet (Blandford & Konigl 1979; Hjellming & Johnston 1988). On the other hand, the radio emission from the jet is quenched in the soft state (Corbel & Fender 2002; Russell et al. 2011). During the transition to the soft state in the outburst rise, bright relativistic flares with optically thin radio spectra are sometimes observed (see Fender & Gallo 2014, and references therein).

Two important aspects of the relation between X-ray spectral and timing properties and the jets are understanding the conditions in the accretion environment for the formation of compact jets (Kalemci et al. 2013, and references therein), and whether jets affect the X-ray spectral and timing properties by altering the accretion environment. One way of achieving these objectives is characterizing the X-ray spectral evolution along with the OIR and radio evolution during outburst decays because the jet emission that is quenched during the soft state turns back on as the source makes a transition to the hard state.

Such multiwavelength characterization during the outburst decays reveal OIR flares (also called "secondary maxima") when the source is back in the hard state with the X-ray spectrum close to its hardest level (Buxton & Bailyn 2004; Kalemci et al. 2005; Coriat et al. 2009; Russell et al. 2010; Dinçer et al. 2012; Buxton et al. 2012; Kalemci et al. 2013). In the 2011 decay of GX 339−4, simultaneous radio and OIR observations show that the OIR flare corresponds to a transition in radio from optically thin to optically thick emission (Corbel et al. 2013b,a). Moreover, the spectral energy distributions (SED) created from data during the OIR flares of 4U 1543−47 (Buxton & Bailyn 2004; Kalemci et al. 2005), and XTE J1550−564 (Jain et al. 2001; Russell et al. 2010) are consistent with emission from a compact jet. A study by Kalemci et al. (2013) showed that the multi-wavelength behavior of most GBHTs that undergo a soft to hard state transition during the outburst decay are similar, such that a compact, steady jet is formed 6-15 days after the initial changes in timing properties, and the jet manifests itself either as an OIR flare, and/or radio emission with flat to inverted spectrum. Alternative explanations for these OIR flares exist, such as the synchrotron emission from a hot accretion flow (Veledina, Poutanen & Vurm 2013; Poutanen & Veledina 2013), and irradiation induced secondary mass accretion which could explain the secondary OIR flares with simultaneous X-ray flares (Kalemci et al. 2013).

To understand the effects of the jet on the X-ray spectral properties, we started a program with the *INTEGRAL* observatory to characterize the GBHTs at high energies when compact jets are present (or while they form). Thermal Comptonization models that are often invoked to explain the high energy behavior of GBHTs predict a cut-off in the X-ray spectrum at a few hundred keVs (Gilfanov 2010). While such cut-offs are observed commonly in many GBHTs, in some cases these cut-offs disappear after the jets turn on
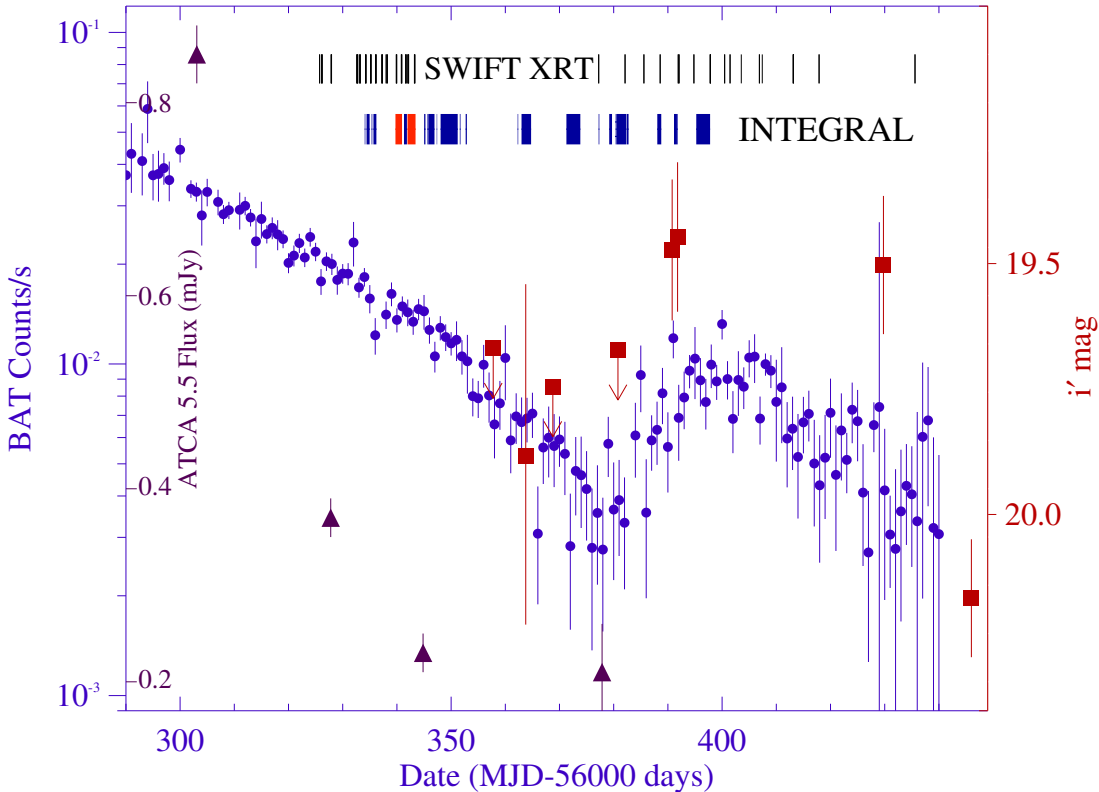
**Figure 2.** Multi-wavelength observations used in this work. Blue solid circles represent *Swift* BAT count rate, solid orange squares are i′ magnitudes (from FTS and RTT 150), purple solid triangles are ATCA radio fluxes at 5.5 GHz. The black short lines at the top represent the times of *Swift* pointed observations. The regions below the *Swift* observations are the times for which the source is within 10° of the INTEGRAL pointing direction. The lighter region (red in the coloured version) represents dedicated *INTEGRAL* observations (PI Kalemci).

(such as in 4U 1543−47, Kalemci et al. 2005), or are not present at all while the jets are present (H1743−322 during 2003 decay, Kalemci et al. 2006a; GX 339−4during the 2005 outburst, Kalemci et al. 2006b; XTE J1720−318, Cadolle Bel et al. 2004; GRO J1655−40 during the 2005 decay, Caballero García et al. 2007, but also see Joinet, Kalemci & Senziani 2008). This disappearance could be interpreted as the jet changing the electron energy distribution and hardening the X-ray spectrum.

Synchrotron emission from compact jets may also be contributing to hard X-rays (Markoff, Falcke & Fender 2001; Markoff, Nowak & Wilms 2005; Maitra et al. 2009; Russell et al. 2010), and both Comptonization and jet models can fit the spectra equally well (Nowak et al. 2011). According to Pe'er & Markoff (2012), a distinct feature of synchrotron radiation at hard X-rays would be a photon index of around 1.5 before a gradual break in the spectrum at ∼10 keV caused by rapid cooling of electrons. Characterizing properties of spectral breaks at hard X-rays therefore is important to test predictions of jet models, especially when these models incorporate detailed electron acceleration mechanisms

Using HEXTE on *RXTE*, Miyakawa et al. (2008) investigated the relation between the cut-off energy (from the fits with cut-off power-law) and several other spectral parameters from all hard state observations of GX 339−4, and found an inverse correlation between the cut-off energy and luminosity for the bright hard state observations. The statistics

were not good enough to constrain the evolution of the cut-off parameters for the fainter observations. Motta, Belloni & Homan (2009) utilized *INTEGRAL* ISGRI and HEXTE together and investigated the evolution of the cut-off energy from the hard state to the hard intermediate state in the rising phase of the outburst of GX 339−4 during the 2006/2007 outburst. Similar to findings of Miyakawa et al. (2008), the cut-off energy decreased with increasing flux, but it reversed the trend and increased again with the softening in the hard-intermediate state. While the cause of this behavior is not clear, obtaining the evolution of spectral breaks during the outburst decay, and comparing with the outburst rise could help us to uncover the reason. Since the hard X-ray fluxes during the outburst decays are lower, dedicated observing programs with *INTEGRAL* are required for such investigation.

Within our *INTEGRAL* program, we first observed XTE J1752−223 with *INTEGRAL*, *Swift* and *RXTE* during its 2012 outburst decay (Chun et al. 2013). The observation took place a few days before the detection of the compact core with the Very Long Baseline Array (VLBA). To increase the statistics of the X-ray spectra at high energy we combined all available ISGRI data, and the resulting spectrum required a break in the hard X-ray spectrum. As a continuation of our observing program with *INTEGRAL*, we triggered on Swift J1745−26 during its decay in 2013.

**Table 1.** *INTEGRAL* observation details

| ISGRI Rev[a] | Dates MJD-56000 | Swift ObsID[b] | ISGRI Exposure (ks) | Avg. offset[c] |
|---|---|---|---|---|
| 1261 | 334.0−335.0 | 00032700005 | 61.0 | 3.93° |
| 1262 | 335.3−336.2 | 00032700007 | 48.0 | 5.19° |
| 1263 | 339.7−340.9 | 000327000010 | 103.7 | 4.18° |
| 1264 | 341.3−343.4 | 000327000013 | 151.9 | 4.82° |
| 1265 | 345.0−346.9 | - | 35.0 | 6.18° |
| 1266 | 347.3−349.8 | - | 20.8 | 5.31° |
| 1267 | 351.0−352.9 | - | 29.2 | 5.94° |
| 1271 | 362.2−364.8 | - | 27.3 | 6.05° |
| 1274 | 371.2−373.2 | - | 22.7 | 6.17° |
| 1276 | 377.2−379.7 | 00533836047 | 104.0 | 5.27° |
| 1277 | 380.2−382.7 | - | 184.2 | 6.34° |
| 1279 | 388.0−388.8 | 00032700017 | 61.8 | 4.85° |
| 1280 | 391.1−391.8 | 00032700018 | 44.9 | 5.13° |
| 1282 | 395.2−397.8 | 00533836049 | 129.5 | 8.50° |

[a] ISGRI Revolution
[b] Swift observation within the given revolution
[c] Average offset of ISGRI pointings

We also obtained data from *INTEGRAL* revolutions before and after our observation.

## 1.1 Swift J1745−26

Swift J1745−26 (Swift J174510.8−2624) was discovered by the BAT instrument on board the *Swift* satellite on September 16 2012 (MJD 56186.39, Cummings et al. 2012). It was subsequently detected by the *Swift* XRT (Sbarufatti et al. 2012), and *INTEGRAL* (Vovk et al. 2012). The infrared counterpart was identified by Rau et al. (2012). Based on the X-ray spectral and timing properties, Swift J1745−26 is reported to be a Galactic black hole transient (Belloni et al. 2012; Tomsick, Del Santo & Belloni 2012). Further evidence for the nature of the source comes from optical observations that reveal a broad, double peaked $H_\alpha$ emission line whose properties resemble those typically seen in other black hole sources in outburst (de Ugarte Postigo et al. 2012; Muñoz-Darias et al. 2013).

Swift J1745−26 is also detected in radio both with the Karl G. Jansky Very Large Array (VLA, Miller-Jones & Sivakoff 2012) and at the Australia Telescope Compact Array (ATCA, Corbel et al. 2012). The spectral index of radio observations during the initial hard state is consistent with optically-thick synchrotron emission from a partially self-absorbed compact jet (Corbel et al. 2012). Curran et al. (2014) present detailed analysis of radio data from ATCA, VLA and Karoo Array Telescope (KAT-7) monitoring observations of Swift J1745−26 until MJD56380. After the initial hard state rise, the source stayed in the hard intermediate state until MJD 56270 based on X-ray spectral and timing properties (Belloni et al. 2012; Grebenev & Sunyaev 2012) and also radio emission properties (Curran et al. 2014). Detailed *Swift* and *INTEGRAL* analysis of the outburst rise is in preparation (Del Santo et al.).

Due to the proximity of the source to the Sun, the source could not be observed between MJD 56270 and MJD 56288 with *Swift* BAT, and the first pointed observation of the source with *Swift* XRT after the gap was on MJD 56334. As shown in Figure 1 of Curran et al. (2014), the system was in the hard intermediate state at MJD 56250 as indicated by the inverted spectrum radio emission. The BAT flux shows an increasing trend after this date, indicating that the spectrum remained hard until the start of the Sun gap on MJD 56270. After a gap of 18 days, the BAT light curve before the break smoothly connects to the light curve after the break. The radio spectrum taken on MJD 56304 and the X-ray spectra on MJD 56334 (Sbarufatti et al. 2013) show that the source is in the hard state after the break. This can also be seen in the hardness-intensity diagram given in Figure 1, where the red data points represent observations analyzed in this work. While we cannot rule out the possibility that the source entered the soft state between MJD 56270 and MJD 56304, the trends in the *Swift* BAT light curve and the radio evolution indicate a "failed" outburst. We note that, while the properties of the source are consistent with the definition of failed outbursts, the outburst certainly did not fail in terms of brightness, and had reached close to a Crab during the initial rise (Sbarufatti et al. 2012).

Finally, the source exhibited a secondary flare after MJD 56380 in optical and X-rays (Russell et al. 2013a). Thanks to the large field of view of *INTEGRAL* and the position of the source in the Galactic Bulge, we were able to analyse *INTEGRAL* data from several revolutions to characterise the high energy behaviour of the source over 70 days during its decay. In this article, we first present the X-ray evolution of the source using both *INTEGRAL*, and *Swift*. Then we discuss the secondary flare observed in both optical and X-ray and compare this flare with the secondary OIR flares observed in GBHTs.

## 2 OBSERVATIONS AND ANALYSIS

### 2.1 X-ray observations

A summary plot of all multi-wavelength observations during the decay can be found in Figure 2. The source has been covered very well with *Swift* and *INTEGRAL*. Our analysis includes *Swift* data between MJD 56334.23 and MJD 56435.59, and *INTEGRAL* data between MJD 56334.0 and MJD 56397.8. The details of the *INTEGRAL* revolutions we utilized and simultaneous *Swift* ObsIDs are given in Table 1.

### 2.2 Spectral extraction with *Swift* XRT, *INTEGRAL* ISGRI and JEM-X

The *Swift* XRT observations used in this study are shown in Table 2. All data were processed following the standard procedures and using the *xrtpipeline v.0.12.8*. Since the source flux varies significantly, the whole sample of pointings contain both Windowed Timing (WT) mode and Photon Counting (PC) mode data. In order to minimise the affects of photon pile-up we followed the method outlined in Reynolds & Miller (2013) and created source selection regions based on the observed count rate. The background region was selected from an annulus with an inner and outer radius of 70" and 100", respectively, from the source centroid. Events were selected with grades 0-2 and 0-12 for WT and PC mode data, respectively. The appropriate response matrix files, swxwt0to2s6_20010101v014.rmf for the WT mode and swxpc0to12s6_20010101v013.rmf for the PC mode, were obtained from HEASARC CALDB. The auxiliary response matrix files were created using the HEASOFT tool *xrtmkarf* and the exposure map created by the *xrtexpomap*. Finally we grouped all the spectra to have at least 50 counts per spectral bin. After the pile-up mitigating procedure, the PC mode observations resulted in a spectrum with few energy bins and large errors, and therefore are not used in this work.

The *INTEGRAL* data were reduced and analyzed using the standard Off-line Scientific Analysis (OSA) software package (v.10) released by the ISDC (Courvoisier et al. 2003) for each revolution. The *INTEGRAL* revolutions last ∼3 days, and within revolutions sky regions are observed with 30-60 minute individual pointings with a special dither pattern to minimise noise in mosaic images obtained by combining images from individual pointings.

For JEM-X, we combined images in a single mosaic per revolution in order to reach the highest sensitivity for JEM X-1 and JEM X-2 separately. The spectra were extracted from the each combined mosaic image over an energy range of 3-35 keV corresponding to 16 channels. After comparing the quality of spectra, we have decided to use only JEM X-1 data. In the case of IBIS/ISGRI, the standard procedure was used to extract the spectra and rebin the response matrix to 50 bins. Then we used *spe_pick* tool to obtain average spectrum of the source for each revolution for 18-350 keV energy range.
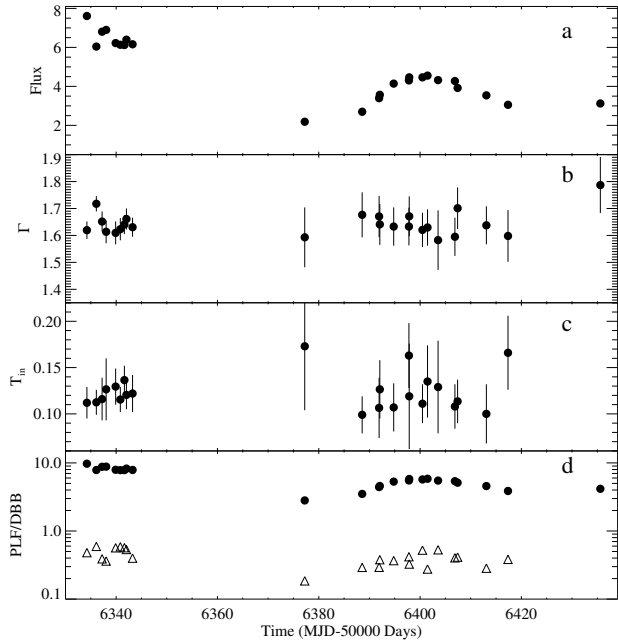


**Figure 3.** Plot of X-ray spectral parameters of *Swift* XRT data only, fitted with a power-law+diskbb model, interstellar absorption (tbabs) with $N_H$ fixed to $2.18 \times 10^{22} cm^{-2}$. a: 1-12 keV flux in units of $10^{-10}$ ergs cm$^{-2}$ s$^{-1}$. b: power-law photon index, c: diskbb inner disk temperature in keV, d: PLF (solid circle) is the power law flux and DBB (triangle) is the diskbb flux in units of $10^{-10}$ ergs cm$^{-2}$ s$^{-1}$ in 1-12 keV band.

### 2.3 X-ray spectral analysis

We first fitted *Swift* XRT and *INTEGRAL* ISGRI spectra separately. For the *Swift* XRT fits, we started with interstellar absorption (*tbabs* in XSPEC) and a power-law. We used cross sections of Verner et al. (1996) and abundances of Wilms, Allen & McCray (2000) for the interstellar absorption and left $N_H$ as a free parameter initially. We observed significant residuals at energies less than 2 keV. We added a multicolor disk blackbody (*diskbb* in XSPEC, Makishima et al. 1986) which resulted in fits with acceptable reduced $\chi^2$ values. The results of the fits are tabulated in Table 2[1]

For the initial, high flux, high quality spectra between MJD 55633.4 and MJD 55644.3, we realized that fits result in a small scatter of $N_H$ values around an average of $2.18 \times 10^{22}$ atoms cm$^{-2}$. Lower quality spectra showed large scatter in $N_H$ that correlated with disk fit parameters. Since it is unlikely that $N_H$ varies more than 20% within timescale of days, we fixed its value to $2.18 \times 10^{22}$ atoms cm$^{-2}$ and performed the fits again. The results show a smooth evolution of X-ray spectral parameters as seen in Figure 3 and in Table 2.

For the *INTEGRAL* observations, we first fitted the ISGRI data from individual revolutions. We started with a power-law, and added a high energy cut off component (*highecut* in XSPEC) and test if addition of the cutoff significantly improves the $\chi^2$. If an *F-test* results in chance

---

[1] All errors in the figures and in tables correspond to $\Delta\chi^2$ of 2.706.

**Table 2.** Swift XRT only fit results

| Swift obsid | Date[a] | Fits with free $N_H$ | | | Fits with $N_H$ fixed | | | |
| | | $N_H$[b] | $\Gamma$ | $T_{in}$ | $\Gamma$ | $T_{in}$ | Flux[c] | Norm[d] |
|---|---|---|---|---|---|---|---|---|
| 00032700005 | 334.2 | 2.12±0.23 | 1.60±0.07 | 0.10±0.02 | 1.62±0.03 | 0.11±0.02 | 7.61±0.10 | >1.07E+06 |
| 00032700007 | 336.1 | 2.08±0.24 | 1.68±0.08 | 0.11±0.02 | 1.72±0.03 | 0.11±0.01 | 6.04±0.09 | >1.64E+06 |
| 00032700008 | 337.2 | 2.14±0.27 | 1.64±0.08 | 0.11±0.03 | 1.65±0.04 | 0.12±0.02 | 6.81±0.08 | >2.41E+05 |
| 00032700009 | 338.0 | 1.88±0.15 | 1.53±0.06 | 0.07±0.03 | 1.61±0.04 | 0.13±0.03 | 6.90±0.08 | >1.15E+05 |
| 00032700010 | 339.9 | 2.08±0.30 | 1.58±0.08 | 0.12±0.03 | 1.61±0.04 | 0.13±0.02 | 6.22±0.09 | >3.00E+05 |
| 00032700011 | 341.6 | 2.44±0.27 | 1.70±0.07 | 0.14±0.01 | 1.64±0.04 | 0.14±0.02 | 6.12±0.07 | >2.52E+05 |
| 00032700012 | 340.8 | 2.41±0.28 | 1.69±0.09 | 0.12±0.01 | 1.62±0.04 | 0.12±0.01 | 6.14±0.09 | >1.27E+06 |
| 00032700013 | 342.0 | 2.26±0.26 | 1.68±0.08 | 0.12±0.02 | 1.66±0.04 | 0.12±0.02 | 6.39±0.09 | >6.83E+05 |
| 00032700014 | 343.2 | 2.22±0.27 | 1.64±0.07 | 0.12±0.02 | 1.63±0.04 | 0.12±0.02 | 6.16±0.06 | >3.52E+05 |
| 00533686047 | 377.2 | 1.64±0.23 | 1.49±0.13 | - | 1.59±0.11 | 0.17±0.07 | 2.19±0.07 | >2.10E+04 |
| 00032700017 | 388.6 | 2.76±0.55 | 1.85±0.19 | 0.10±0.02 | 1.68±0.08 | 0.10±0.02 | 2.70±0.09 | >1.59E+06 |
| 00032700018 | 391.9 | 2.29±0.52 | 1.69±0.17 | 0.10±0.04 | 1.67±0.08 | 0.11±0.03 | 3.39±0.11 | >3.14E+05 |
| 00533836048 | 392.1 | 2.36±0.55 | 1.68±0.16 | 0.12±0.03 | 1.64±0.08 | 0.13±0.03 | 3.57±0.09 | >1.18E+05 |
| 00032700019 | 394.8 | 2.21±0.46 | 1.63±0.15 | 0.10±0.03 | 1.63±0.07 | 0.11±0.03 | 4.14±0.10 | >6.08E+05 |
| 00533836049 | 397.8 | 3.28±0.66 | 1.86±0.15 | 0.15±0.02 | 1.63±0.07 | 0.16±0.03 | 4.31±0.12 | >2.10E+04 |
| 00032700020 | 397.9 | 1.92±0.33 | 1.59±0.13 | 0.08±0.06 | 1.67±0.07 | 0.12±0.06 | 4.47±0.12 | >4.50E+05 |
| 00032700021 | 400.5 | 2.66±0.49 | 1.74±0.14 | 0.11±0.02 | 1.62±0.06 | 0.11±0.02 | 4.46±0.10 | >9.16E+05 |
| 00533836050 | 401.5 | 2.74±0.55 | 1.76±0.15 | 0.14±0.03 | 1.63±0.07 | 0.13±0.04 | 4.55±0.11 | >4.06E+05 |
| 00032700022 | 403.6 | 2.37±0.88 | 1.62±0.25 | 0.11±0.07 | 1.58±0.11 | 0.13±0.05 | 4.32±0.19 | >5.39E+05 |
| 00032700023 | 406.9 | 2.84±0.53 | 1.77±0.16 | 0.11±0.02 | 1.60±0.07 | 0.11±0.02 | 4.28±0.12 | >6.76E+05 |
| 00533836051 | 407.4 | 2.35±0.49 | 1.75±0.16 | 0.11±0.02 | 1.70±0.08 | 0.11±0.02 | 3.92±0.11 | >5.14E+05 |
| 00533836052 | 413.1 | 2.23±0.47 | 1.64±0.16 | 0.09±0.04 | 1.64±0.07 | 0.10±0.03 | 3.54±0.09 | >5.00E+05 |
| 00533836053 | 417.4 | 2.20±0.00 | 1.60±0.10 | 0.17±0.04 | 1.60±0.10 | 0.17±0.04 | 3.06±0.10 | >1.43E+05 |
| 00533836057 | 435.6 | 3.14±1.08 | 2.01±0.32 | 0.08±0.06 | 1.79±0.10 | - | 3.12±0.13 | - |

[a] MJD-56000
[b] in units of $10^{22}$ atoms cm$^{-2}$
[c] 1-12 keV Flux in units of $10^{-10}$ ergs cm$^{-2}$ s$^{-1}$
[d] Lower limit of normalization of *diskbb* component

probability less than 0.001, we used the fit with the cutoff. The fit results are summarized in Table 4 and some of the fit parameters are plotted in Figure 4.

Finally, we applied joint fits to the *Swift* XRT, *INTEGRAL* ISGRI and JEM-X for observations with concurrent data (Table 1). We started with a model that consists of power-law and multicolor diskblackbody components with interstellar absorption. Similar to ISGRI-only fits, we add a high energy cut-off and check the improvement in $\chi^2$. If an *F-test* results in chance probability less than 0.001, we used the fit with the cutoff.

We also applied thermal and hybrid Comptonization models to the joint spectra. In the *compps* model (Poutanen & Svensson 1996), blackbody photons are Compton up-scattered from a spherical corona with uniform optical depth $\tau_y$ and electron temperature $kT_e$. In our fits, the blackbody temperature is fixed to the *diskbb* inner temperature $T_{in}$. We kept all other parameters at default values. The fits cannot constrain the reflection fraction.

Finally, we tried the *eqpair* model (Coppi 1999) to be able to assess the presence of non-thermal electron population. The *eqpair* model assumes a spherical plasma of electrons, positrons and soft photons. The resulting emission is determined by the compactness parameter $l = L\sigma T/Rm_e c^3$, where $L$ is power, $R$ is the radius of the spherical plasma, and $\sigma_T$ is the Thomson cross section. The model allows hybrid electron plasmas, thermal and non-thermal electron energy distributions together. Following Coppi (1999), we fixed the

**Table 3.** Optical Magnitudes

| Date | $i'$ | $R$ | $V$ |
|---|---|---|---|
| 56357.8 | >19.67 | >20.75 | >19.73 |
| 56363.8 | 19.88±0.34 | 20.92±0.35 | >21.13 |
| 56368.8 | >19.74 | 20.67±0.24 | >21.19 |
| 56380.8 | >19.67 | >20.83 | >20.39 |
| 56390.8 | 19.47±0.14 | 20.72±0.25 | >20.83 |
| 56391.8 | 19.45±0.15 | 20.45±0.21 | 21.58±0.48 |
| 56429.8 | 19.50±0.14 | 20.20±0.13 | 22.94±0.55 |
| 56441.8 | >18.67 | >20.36 | 21.04±0.55 |
| 56451.8 | >18.98 | >20.49 | >21.97 |
| 56537.4 | >20.78 | - | >21.26 |
| 56446[a] | 20.07±0.12 | - | - |

[a] From Grebenev, Prosvetov & Burenin (2014)

soft photon compactness $l_s$ to 1, and fit our data with a minimum set of free parameters. The temperature of seed photons are fixed to the inner disk temperature of the *diskbb* component. The fit results for Comptonization models are summarized in Table 5. An example fit is shown in Figure 5.

## 2.4   Radio and optical data

During the decay, the source was also monitored in radio and in optical. There were four radio observations with the ATCA, and for all those observations the radio spectra are consistent with being flat to inverted, indicating presence of compact jets (Curran et al. 2014).

Optical observations were acquired using the Faulkes Telescope South (FTS; located at Siding Spring, Australia) as part of a monitoring campaign of $\sim 30$ LMXBs with the Faulkes Telescopes (Lewis et al. 2008). Three filters were used, Sloan Digital Sky Survey (SDSS) i′, Bessell R and Bessell V. Bias subtraction and flat-fielding were performed via the automatic pipelines. For flux calibration procedures, see Muñoz-Darias et al. (2013). The magnitudes in each band are given in Table 3. We also take one i′ band magnitude measured on MJD 56446 taken at Turkish National Observatory with Russian Turkish Telescope RTT150 reported in Grebenev, Prosvetov & Burenin (2014).

## 3   RESULTS

### 3.1   Soft X-ray evolution with *Swift* XRT

As mentioned earlier, leaving $N_H$ free results in highly scattered, and correlated $N_H$ and *diskbb* parameters. In some cases the *diskbb* flux changes by an order of magnitude within a day. After fixing the $N_H$, a smooth evolution of X-ray spectral fit parameters is observed (Figure 3).

A soft *diskbb* component is required statistically in the fits, however, its parameters are not very well determined, especially the normalization. The 90% confidence lower limits on the *diskbb* normalisations are given in Table 2 along with other important fit parameters. The minimum normalizations typically are larger than a few times $10^5$, and the lowest we measure is $10^4$. While the quality of the data is not good enough to place strong constraints on the inner disk radius, for typical black hole masses and distances, these minimum normalization values indicate large inner disk radii.

The 1-12 keV X-ray flux decreases from $8 \times 10^{-10}$ ergs cm$^{-2}$ s$^{-1}$ to $2 \times 10^{-10}$ ergs cm$^{-2}$ s$^{-1}$ in $\sim$43 days before showing a flare. The flare lasts for approximately 40 days. As seen in Figure 2, the flare occurs in both soft and hard X-rays. The flare causes an increase of flux in both *diskbb* and power-law flux, and the photon indices remain remarkably constant even though the soft X-ray flux more than doubles during the flare.

### 3.2   Hard X-ray evolution and joint fits

The evolution of the hard X-ray flux with BAT is shown in Figure 2, and the evolution of the spectral fit parameters of *INTEGRAL* ISGRI data only are given in Table 4. We were able to search and detect cut-offs in the ISGRI data for revolutions with high flux (1261 to 1265), and also during the final revolution (1282) for which the source was in the field of view of *INTEGRAL*. For revolution 1282, the statistical quality of the spectrum is better than for revolutions 1266 to 1280 because of higher exposure as well as higher flux due to the observation occurring near the peak of the X-ray flare.

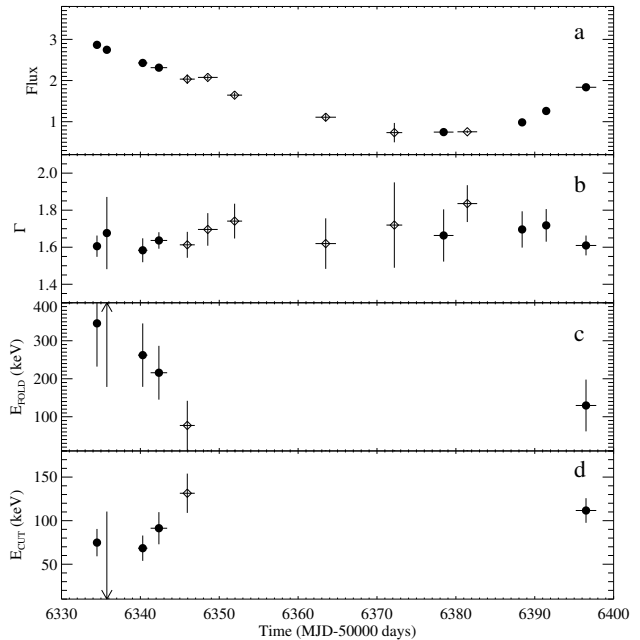For *INTEGRAL* revolutions with simultaneous *Swift*



**Figure 4.** Evolution of spectral fit parameters from a with a power-law and a cut-off. Filled circles are joint fits to *INTEGRAL* ISGRI and *Swift* XRT (therefore the model also includes *diskbb*), and empty diamonds are fits to only ISGRI spectra. a: 13-200 keV flux in units of $10^{-9}$ ergs cm$^{-2}$ s$^{-1}$. b: photon index. c: Folding Energy and d: Cut-off energy of the *highec* model, respectively.

XRT data we applied joint fits with three models; phenomenological *highec\*(power+diskbb)*, and Comptonization models *compps+diskbb* and *eqpair+diskbb*. For revolutions 1261, 1263, 1264 and 1282, a cut-off is required in the power-law model fit (see Table 5). The evolution of spectral parameters related to hard X-rays is summarized in Fig. 4. In this figure we used solid circles to represent joint fit results, and used diamonds from ISGRI only fits for which we do not have XRT data.

At first instance, fits from the earliest five revolutions seem to have a harder photon index compared to later revolutions, however this is an artificial result due to the presence of a cut-off in the spectra of earlier revolutions. This evolution indicates that it is likely that the data from revolutions 1266 to 1280 also require a high energy cut-off, however since it is not required by the *F-test* due to low statistics, the cut-off is not included in the fits and the resulting power-law index is softer.

The evolution of folding and cut-off energies indicate that as the flux decayed initially, the cut-off energies increased and folding energies decreased. The high cut-off, low folding energy behavior was also observed during the peak of the secondary flare during revolution 1282.

For the *compps* fits, we first let electron temperature, $y-parameter$ ($\tau_y$), and reflection fraction free. For all observations, the reflection fraction is close to zero and could not be constrained by the fits. We then fixed this parameter to zero, and fitted the spectra with electron temperature and $\tau_y$ as free parameters (see Table 5 for results). We find electron temperatures of 60-100 keV for the revolutions 1261 to 1264. The electron temperature at revolution 1282 is higher, but

**Table 4.** ISGRI only fit results

| ISGRI Rev | $\Gamma$ | $E_{fold}$[a] (keV) | $E_{Cut}$[b] (keV) | Flux[c] |
|---|---|---|---|---|
| 1261 | 1.55±0.06 | 273.6± 94.6 | 68.9± 12.6 | 2.82±0.07 |
| 1262 | 1.45±0.20 | <110.5 | >178.6 | 2.63±0.09 |
| 1263 | 1.56±0.06 | 255.9± 82.3 | 65.7± 16.7 | 2.37±0.04 |
| 1264 | 1.60±0.04 | 220.3± 62.0 | 81.2± 13.4 | 2.30±0.03 |
| 1265 | 1.61±0.07 | $33.0^{+109.1}_{-21.3}$ | $140.8^{+13.2}_{-31.9}$ | 2.03±0.11 |
| 1266 | 1.70±0.09 | - | - | 2.08±0.07 |
| 1267 | 1.74±0.09 | - | - | 1.65±0.06 |
| 1271 | 1.62±0.14 | - | - | 1.11±0.09 |
| 1274 | 1.72±0.23 | - | - | 0.74±0.24 |
| 1276 | 1.74±0.14 | - | - | 0.71±0.05 |
| 1277 | 1.84±0.10 | - | - | 0.76±0.03 |
| 1279 | 1.72±0.10 | - | - | 0.97±0.04 |
| 1280 | 1.78±0.09 | - | - | 1.22±0.04 |
| 1282 | 1.64±0.05 | 131.8± 71.5 | 114.2± 15.4 | 1.83±0.05 |

[a] Folding energy in *highecut* model
[b] Cut-off energy in *highecut* model
[c] 13-200 keV Flux in units of $10^{-9}$ ergs cm$^{-2}$ s$^{-1}$

with large errors. We cannot constrain the $\tau_y$ with *compps* fits, within $\Delta\chi^2$ of 2.706, the $\tau_y$ parameter is pegged to the upper limit of 3.

For the *eqpair* fits we started with fixing $l_{nt}/l_h$ to zero to see if the thermal electron distribution can fit the data. We only had $l_h/l_s$ (hard to soft compactness ratio) and $\tau_p$ free and fixed all the other parameters. After we obtained initial fits, we let reflection fraction vary. Like the *compps* case, for all revolutions, the fits resulted in reflection fractions close to zero. We fixed it to zero and repeated the fits. The results are given in Table 5.

We then tested whether a hybrid electron energy distribution provides better fit to the data. We made $l_{nt}/l_h$ a free parameter and fixed $\Gamma_{inj}$ to 2.5. While the fits cannot constrain the $l_{nt}/l_h$ parameter well enough to rule out non-thermal plasma, we consistently obtain low values of $l_{nt}/l_h$ for all revolutions, except revolution 1262. The $2\sigma$ limits for this parameter are given in Table 5. Except revolution 1262 $l_{nt}/l_h$ values are consistent with zero, and the $l_h/l_s$ and $\tau_p$ parameters for the non-thermal fits are very similar to the thermal fits. Therefore, in Table 5 we only show thermal fit results for these parameters.

## 4   DISCUSSION

### 4.1   The origin of the flare in X-rays and optical

The secondary flare is clearly visible at hard X-ray and optical wavelengths, starting around MJD $\sim$ 56380 and ending by MJD $\sim$ 56440 (Figure 2). Flares in optical and infrared are common during the decays of GBHTs. These flares can be attributed to formation of compact jets (Kalemci et al. 2013, and references therein), synchrotron radiation from hot accretion flows (Poutanen & Veledina 2013, and references therein) and enhanced mass accretion from outer disk or the companion as a response to heating from primary

(Augusteijn, Kuulkers & Shaham 1993; Zurita et al. 2002; Ertan & Alpar 2002).

Being likely a failed outburst, Swift J1745−26 did not go through a soft state, and even at the beginning of the decay, the radio emission from the compact jet was present as indicated by the flat to inverted radio spectra from ATCA observations (see Figure 2). While the radio emission is present, whether we could observe infrared emission at the same time depends on the evolution of the break in the jet SED. In MAXI J1836–194, which also performed a failed outburst, the jet never quenched at radio frequencies, but the break in the spectrum between optically thin and partially self-absorbed (flat / inverted) synchrotron emission moved from the mm regime to the infrared regime as the source made a transition back to the hard state. This indicated an increase in the jet power as the source entered the hard state, resulting in a flare in the infrared and optical emission (Russell et al. 2013b, 2014). Similar evolution may be occurring in Swift J1745−26, whereby the late flare could be a result of break frequency moving towards the infrared. However, the flare in MAXI J1836–194 peaked within a few days of the transition to the hard state, as did the flare of GX 339−4 in 2011 (Corbel et al. 2013a). Kalemci et al. (2013) have shown that the infrared flares usually peak about 10-20 days after the source has fully entered the hard state. The late optical and X-ray re-brightening of Swift J1745−26 occurred about 100 days after the transition to the hard state, which is therefore substantially delayed compared to these synchrotron jet flares. Unfortunately we do not have optical coverage within days of the transition to the hard state, so we do not know if there was an additional optical/infrared flare at that time. The hot accretion flow is also an unlikely explanation for the flare, as throughout the decay that lasts for more than 100 days, there is no significant change in the properties of hard X-rays, and it is difficult to explain why the synchrotron emission suddenly turns on 80 days after the start of the decay.

**Table 5.** joint fit results

| | | High Energy Cut-off Fits | | | |
|---|---|---|---|---|---|
| ISGRI Rev | $\Gamma$ | $E_{Fold}$ | $E_{Cut}$ | Flux[a] | $\chi^2$/DOF |
| 1261 | 1.61±0.02 | 345.8±113.9 | 74.8± 15.7 | 3.69±0.05 | 407.4/357 |
| 1262 | 1.68±0.03 | - | - | 3.422±0.05 | 310.4/284 |
| 1263 | 1.58±0.01 | 262.2± 83.5 | 68.4± 14.5 | 3.10±0.07 | 235.0/269 |
| 1264 | 1.64±0.03 | 215.8± 70.8 | 91.3± 18.4 | 3.00±0.04 | 295.5/275 |
| 1276 | 1.66±0.03 | - | - | 0.98±0.05 | 96.4/ 88 |
| 1279 | 1.70±0.06 | - | - | 1.26±0.05 | 89.0/ 94 |
| 1280 | 1.72±0.06 | - | - | 1.61±0.04 | 122.0/111 |
| 1282 | 1.61±0.04 | 129.6± 68.2 | 111.6± 14.1 | 2.30±0.05 | 179.7/135 |

| | Compps Fits | | |
|---|---|---|---|
| ISGRI Rev | $kT_e$ (keV) | $\tau_y$ | $\chi^2$/DOF |
| 1261 | 73.5±13.4 | $3^{+0}_{-0.93}$ | 409.0/358 |
| 1262 | 92.9±23.9 | $3^{+0}_{-1.60}$ | 317.8/283 |
| 1263 | 66.3± 8.0 | $3^{+0}_{-0.62}$ | 239.7/270 |
| 1264 | 69.3±11.8 | $3^{+0}_{-0.89}$ | 295.7/276 |
| 1282 | 119.3±60.9 | $3^{+0}_{-2.16}$ | 187.2/136 |

| | | Eqpair Fits[b] | | | |
|---|---|---|---|---|---|
| ISGRI Rev | $\tau_p$ | $l_h/l_s$ | $\chi^2_{ther}$/DOF[c] | $l_{nt}/l_h$[d] | $\chi^2_{hybr}$/DOF[e] |
| 1261 | 2.06± 0.11 | 12.25±1.08 | 406.8/357 | <0.48 | 406.6/356 |
| 1262 | 1.23± 0.24 | 9.99±1.12 | 313.1/282 | >0.39 | 306.5/281 |
| 1263 | 2.03± 0.31 | 11.51±1.10 | 240.5/269 | <0.50 | 240.5/268 |
| 1264 | 1.79± 0.32 | 10.37±0.93 | 294.2/275 | <0.78 | 293.5/274 |
| 1282 | 1.32± 0.70 | 8.29±1.18 | 185.4/135 | <0.57 | 188.8/134 |

[a] 1-200 keV Flux in units of $10^{-9}$ ergs cm$^{-2}$ s$^{-1}$
[b] $l_{bb}$ is fixed to 1., $\Gamma_{inj}$ is fixed to 2.5 and $Refl$ fixed to 0.
[c] $\chi^2$ of thermal electron energy distribution fits, $l_{nt}/l_h=0$.
[d] $2\sigma$ limits
[e] $\chi^2$ of hybrid electron energy distribution fits, $l_{nt}/l_h$ is a free parameter

Independent of the emission mechanism, a late flare could be caused by enhanced mass accretion in response to a previous heating event, which could in principal boost all accretion components at late times (disc emission, hot flow or jet). The event that triggered the enhanced mass accretion for Swift J1745−26 could be the initial outburst that peaked around MJD 56190, or it could be the increase in the hard X-rays observed between MJD 56260 and MJD 56270 which likely correspond to a transition from an intermediate state to the hard state (Curran et al. 2014). Being observed in both X-rays and optical also support that the origin of this flare is enhanced mass accretion. For such a scenario, one would expect the X-rays to lag the optical flare (Ertan & Alpar 2002), however, the optical coverage is insufficient to test this prediction.

Such simultaneous X-ray/OIR flares are observed in other sources. XTE J1752−223 is such a case in which a late flare occurred ∼55 days after the transition to the hard state. Russell et al. (2012) measured the SED optical to X-ray spectral index during the flare to be −1.0±0.3 which is consistent with synchrotron emission from a compact jet. A detailed investigation of SMARTS light curves in the $H$ and $I$ bands show that apart from the large flare with simultaneous enhancement in the OIR and X-rays, there is an earlier, smaller flare observed close to the first detection of the compact core with the VLBA (Chun et al. 2013). Kalemci et al.

(2013) interpreted this smaller flare as corresponding to the formation of compact jet, and large simultaneous X-ray/OIR flare as caused by enhanced mass accretion.

Similar behavior is observed during the decay of GX 339−4 in its 2007 outburst. The OIR flare that started on MJD 54241 is interpreted as formation of the compact jet in Kalemci et al. (2013). The OIR flare, instead of decaying within a few tens of days as in other outbursts of GX 339−4, 4U 1543−47, and XTE J1550−564 (Buxton et al. 2012; Kalemci et al. 2013) lasted for more than 100 days (Dincer et al. 2008). An X-ray flare starts around MJD 52460, that corresponds to a break and a slight increase in the $H$ band flux (See Figure 3 of Dincer et al. 2008).

Based on these observations, we claim that there are two types of secondary maxima of OIR emission in GBHTs during outburst decays. During the formation of the compact jets, combination of increase in jet power and/or increase in the frequency of the SED break results in an increase in the OIR emission. These OIR flares are not accompanied by an increase in X-ray flux, and their properties are discussed in detail in Kalemci et al. (2013). The second type of OIR flare is caused by increased mass accretion due to a previous heating event, and these type of flares are accompanied by an increase in X-ray flux. For some sources only one type flare is observed, and for others (like GX 339−4 in 2007 and
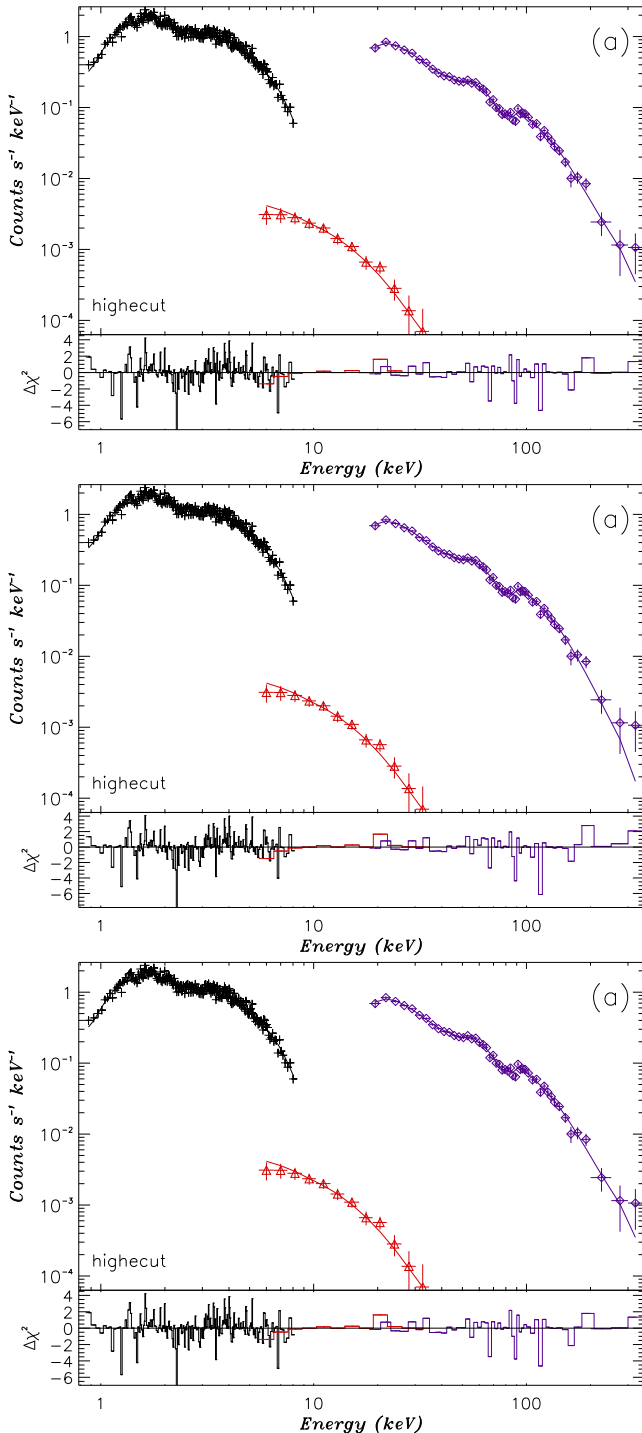
**Figure 5.** Fits to joint *Swift* XRT (crosses, black in colored version), *INTEGRAL* ISGRI (diamonds, purple in colored version) and JEM-X (triangles, red in colored version) spectra for revolution 1263. Fits are with a: *highecut*, b: *comps* and c: *eqpair* model.
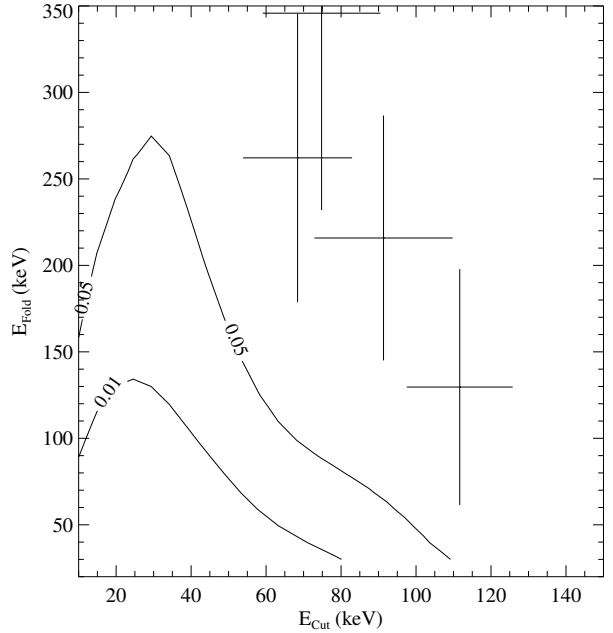


**Figure 6.** Contours of 5% and 1% confidence levels for goodness of fit for the long H1743−322 observation taken with *RXTE* when cut-off and folding energies are varied in the fit. The Swift J1745−26 cut-off and folding energies with errors are over plotted.

state at this time, a mass increase in the disk going towards the black hole may increase the flux of all the accretion components: inner disk, hot flow and the jet. We might obtain some clues about the emission mechanism by investigating the evolution of X-ray spectra as discussed in the next section.

## 4.2    High energy behavior of the source

Thanks to the wide field of view of the *INTEGRAL* ISGRI instrument, and pointed observations with *Swift* XRT, we were able to analyze the broad-band spectral evolution of the source at the beginning of the decay (revolutions 1261-1264), and at the peak of the flare (revolution 1282). We have shown that five revolutions having ISGRI data with good statistical quality require a cut-off in the fit, and we have some evidence (from Γ) that several of the other probably have a cut-off.

### 4.2.1    High energy breaks and jets

Both of the sources we observed with our *INTEGRAL* program, XTE J1752−223 and Swift J1745−26, show presence of a break in the hard X-ray spectrum while the jets are present. This was in contrast to our earlier results from the HEXTE data that indicate disappearance of breaks while the jet turns on. Suspecting that the disappearance of the break is an artifact of the quality of the data, we decided to check the spectra of 4U 1543−47 and H1743−322 during their decays to find which combinations of cut-off and folding energies are statistically acceptable. For both 4U 1543−47 and H1743−322 we found the observations with the best

XTE J1752−223) both can be observed during the same outburst.

While the underlying mechanism causing the simultaneous secondary X-ray/OIR flares might be the increased mass accretion for these sources, this does not by itself reveal the emission mechanism. Since the source is in the hard

statistics, and multiplied the existing fit with the *highecut*. As reported earlier in Kalemci et al. (2005) and Kalemci et al. (2006a), the addition of the break into the spectrum is not statistically significant. We then used *steppar* in XSPEC and varied the cut-off and folding energies and recorded the $\chi^2$ values. We plotted contours of 5% and 1% levels for which the given folding and cut-off values are acceptable. We show the H1743−322 obsid 80137-02-01-01 result as an example in Fig. 6 because it had ∼6 ks of exposure with *RXTE*, and had the best statistics for fitting the spectrum. Even at the 5% level, a large parameter space of folding and cut-off energies can fit the data. To illustrate this point further, we placed the cut-off and break energy combinations of Swift J1745−26 from this work, and all of these combinations would lead to an acceptable fit for the example spectrum of H1743−322 that we discuss. For all other observations with *RXTE* (including observations for 4U 1543−47), the statistics are even worse than the example given, and basically all combinations of cut-off and folding energies are acceptable, except low cut-off (<50 keV) and low folding energy (<100 keV) combinations. Therefore, spectra taken with HEXTE on *RXTE* provide insufficient quality to characterize cut-offs during the decay for typical hard X-ray fluxes. Long *INTEGRAL* monitoring observations are required to understand the relation between the compact jet formation and hard X-ray behavior.

We can compare the behaviour of the spectral breaks of Swift J1745−26 with different sources. For 4U 1543−47, with the formation of the jet, the folding energy and/or the cut-off energy must have increased. For H1743−322, no break was necessary in the fit before the presence of compact jets, and this trend continued after the compact jet is observed, so we do not know the evolution, but we can say that even if there is a break, the cut-off and/or folding energies must be high when the compact jet is present. For Swift J1745−26, we observed an increase in the cut-off energy as the decay progressed during the outburst decay, but we also observed a decrease in the folding energy, resulting in a sharp break in the spectrum. The situation is quite different for XTE J1752−223 where we measured a cut-off energy of $25.3^{+7.3}_{-7.6}$ keV and a folding energy of $236^{+42}_{-32}$ keV (Chun et al. 2013) indicating a smooth, gradual break at high energies. This observation took place when the compact jet was first observed with the VLBA, but before the large secondary flare. Overall, the behavior of Swift J1745−26] and XTE J1752−223 for which we have high quality *INTEGRAL* data do not support the argument that the high energy breaks disappear as the jets turn on.

High energy breaks as discussed in this work is a common feature in models invoking both Comptonization and synchrotron as the source of emission. For the model discussed in Pe'er & Markoff (2012), the electrons at the jet base characteristically produce a power law with a photon index of around 1.5 and a break at higher energies. The location of the break is determined by the acceleration mechanism whose details are uncertain. While Pe'er & Markoff (2012) model can roughly reproduce the spectra for both earlier and later revolutions of Swift J1745−26 (Asaf Peer, personal communication), it cannot place strong constraints on the physical parameters yet.

Recently, based on a broadband observation taken at MJD 56446 at the end of the secondary flare (the last i′ data

in Figure 2), Grebenev, Prosvetov & Burenin (2014) claimed that emission at the time may be dominated by jet emission since a single power-law can fit the entire SED from optical to Gamma-rays. They first take the optical and a single *Swift* BAT flux, and fitted them with a single power-law by modifying the $N_H$. Then they added *Swift* XRT spectra taken 10 days earlier (last observation in Table 2), and showed that the single power-law with an $N_H$ of $1.205 \pm 0.026 \times 10^{22}$ atoms cm$^{-2}$ found from the optical to BAT fit also fits the XRT data. While this result seems intriguing, we do not think that the quality of the data is sufficient for arriving at strong conclusions about the emission mechanism. We have also analysed the same XRT data using their absorption model, and found that the fit gives $N_H = 1.44 \pm 0.29 \times 10^{22}$ atoms cm$^{-2}$ . Therefore errors on both the power-law index and $N_H$ are quite large, and it is not surprising that a single power-law passes through all XRT data.

### 4.2.2 Comptonization models

The behavior of hard X-rays can be well explained by Comptonization for Swift J1745−26. The thermal Comptonization model *compps* fits provide reduced $\chi^2$ values close to 1. Finally, all revolutions, except revolution 1262, can be fitted with the *eqpair* model without requiring a hybrid electron plasma. Therefore, except revolution 1262, the high energy behavior of the source is consistent with thermal Comptonization of disk photons. Fig. 5 show that phenomenological and physical fits all represent the data very well (which is not surprising, see discussion in Coppi 1999).

Even for revolution 1262 a thermal Comptonization model cannot be ruled out given the very small improvement of $\chi^2$ of the hybrid case to that of the thermal case (see Table 5). The *compps* still provides an acceptable fit (reduced $\chi^2$ of 1.123). We added a hard power-law to *compps* fit (following Joinet et al. 2007) to test the presence of additional components due to non-thermal Comptonization. The fitted power-law index was ∼1 (not constrained), and the improvement in the $\chi^2$ was marginal (with an $F - test$ chance probability of 0.008).

While non-thermal electron energy distributions are commonly required in the intermediate and sometimes in the soft states (Del Santo et al. 2008; Gierliński et al. 1999; Malzac et al. 2006), they are rarely required in the hard states, and all claims of non-thermal electron distributions in the hard state are during bright hard states at the outburst rise (Joinet et al. 2007; Droulans et al. 2010; Caballero García et al. 2007; McConnell et al. 2000). Thanks to our *INTEGRAL* observing program, now we obtained high quality data extending above 300 keV for two sources in the hard state during the decay, XTE J1752−223 (Chun et al. 2013) and Swift J1745−26, and for both sources fits are consistent with thermal Comptonization. Continuing dedicated *INTEGRAL* observations of GBHTs during outburst decays is very important to establish patterns in the high energy behavior, and to compare these patterns with the behavior during outburst rise.

## 5   SUMMARY

We characterized the multiwavelength evolution of Swift J1745−26 during the decay of the 2013 outburst using X-ray data from *INTEGRAL* ISGRI, JEM-X and *Swift* XRT, optical observations taken at FTS and TUG and radio observations of ATCA. We fit the X-ray spectra with thermal and hybrid Comptonization models as well as phenomenological models. Our main findings can be summarized as follows:

• We concluded that the physical origin of a flare observed both in optical and X-rays ∼170 days after the peak of the outburst that lasted for ∼50 days is enhanced mass accretion in response to an earlier heating event.

• We showed that a high energy break is needed in the spectra, and for the joint ISGRI-XRT fits, the cut-off energy increased from 75 keV to 112 keV while the folding energy decreased from 350 keV to 130 keV as the decay progresses.

• We investigated the claim that high energy cut-offs disappear with the compact jet turning on during outburst decays, and showed that spectra taken with HEXTE on *RXTE* provide insufficient quality to characterize cut-offs during the decay for typical hard X-ray fluxes. Data taken with *INTEGRAL* do not support the claim of disappearance of spectral breaks.

• We found that for the entire decay (including the flare) the X-ray spectra are consistent with thermal Comptonization, but jet synchrotron origin cannot be ruled out.

## REFERENCES

Augusteijn T., Kuulkers E., Shaham J., 1993, A&A, 279, L13

Belloni T. et al., 2012, The Astronomer's Telegram, 4450

Belloni T. M., 2010, in Lecture Notes in Physics, Berlin Springer Verlag, Vol. 794, Lecture Notes in Physics, Berlin Springer Verlag, T. Belloni, ed., p. 53

Blandford R. D., Konigl A., 1979, ApJ, 232, 34

Brocksopp C., Bandyopadhyay R. M., Fender R. P., 2004, New Astronomy, 9, 249

Buxton M., Bailyn C. D., 2004, ApJ, 615, 880

Buxton M., Bailyn C. D., Capelo H., Chatterjee R., Dincer T., Kalemci E., Tomsick J. A., 2012, AJ, 143, 130

Caballero García M. D. et al., 2007, ApJ, 669, 534

Cadolle Bel M. et al., 2004, A&A, 426, 659

Capitanio F., Belloni T., Del Santo M., Ubertini P., 2009, MNRAS, 398, 1194

Chun Y. Y. et al., 2013, ApJ, 770, 10

Coppi P. S., 1999, in ASP Conf. Ser. 161: High Energy Processes in Accreting Black Hole, eds. Poutanen, J. and Svensson, R.

Corbel S. et al., 2013a, MNRAS, 431, L107

Corbel S., Coriat M., Brocksopp C., Tzioumis A. K., Fender R. P., Tomsick J. A., Buxton M. M., Bailyn C. D., 2013b, MNRAS, 428, 2500

Corbel S., Edwards P., Tzioumis T., Coriat M., Fender R., Brocksopp C., 2012, The Astronomer's Telegram, 4410

Corbel S., Fender R. P., 2002, ApJ, 573, L35

Corbel S., Fender R. P., Tzioumis A. K., Nowak M., McIntyre V., Durouchoux P., Sood R., 2000, A&A, 359, 251

Coriat M., Corbel S., Buxton M. M., Bailyn C. D., Tomsick J. A., Körding E., Kalemci E., 2009, MNRAS, 400, 123

Courvoisier T. J.-L. et al., 2003, A&A, 411, L53

Cummings J. R. et al., 2012, GRB Coordinates Network, 13775

Curran P. A. et al., 2014, MNRAS, 437, 3265

de Ugarte Postigo A., Sanchez-Ramirez R., Munoz-Darias T., Gorosabel J., Thoene C. C., Cabrera-Lavers A., 2012, The Astronomer's Telegram, 4388

Del Santo M., Malzac J., Jourdain E., Belloni T., Ubertini P., 2008, MNRAS, 390, 227

Dinçer T., Kalemci E., Tomsick J. A., Buxton M., Bailyn C., Corbel S., 2012, ApJ, 753, 55

Dincer T., Kalemci E., Tomsick J. A., Buxton M., 2008, in Proceedings of the VII Microquasar Workshop: Microquasars and Beyond, Kalemci E., ed., (Turkey: Foca, Izmir), pp. 61, http://pos.sissa.it/cgi–bin/reader/conf.cgi?confid=62

Droulans R., Belmont R., Malzac J., Jourdain E., 2010, ApJ, 717, 1022

Ertan Ü., Alpar M. A., 2002, A&A, 393, 205

Fender R., 2010, in Lecture Notes in Physics, Berlin Springer Verlag, Vol. 794, Lecture Notes in Physics, Berlin Springer Verlag, T. Belloni, ed., p. 115

Fender R. P., 2001, MNRAS, 322, 31

Fender R. P., Gallo E., 2014, accepted for publication in Space Science Reviews; arXiv:1407.3674

Ferrigno C., Bozzo, E., Del Santo M., Capitanio, F., 2012, A&A, 537, L7

Gierliński M., Zdziarski A. A., Poutanen J., Coppi P. S., Ebisawa K., Johnson W. N., 1999, MNRAS, 309, 496

Gilfanov M., 2010, in Lecture Notes in Physics, Berlin Springer Verlag, Vol. 794, Lecture Notes in Physics, Berlin Springer Verlag, T. Belloni, ed., p. 17

Grebenev S. A., Prosvetov A. V., Burenin R. A., 2014, Astronomy Letters, 40, 171

Grebenev S. A., Sunyaev R. A., 2012, The Astronomer's Telegram, 4401

Homan, J., Wijnands, R., van der Klis, M., Belloni, T., van Paradijs, J., Klein-Wolt, M., Fender, R., Méndez, M., 2001, ApJS, 132, 377

Hjellming R. M., Johnston K. J., 1988, ApJ, 328, 600

Jain R. K., Bailyn C. D., Orosz J. A., McClintock J. E., Remillard R. A., 2001, ApJ, 554, L181

Joinet A., Jourdain E., Malzac J., Roques J. P., Corbel S., Rodriguez J., Kalemci E., 2007, ApJ, 657, 400

Joinet A., Kalemci E., Senziani F., 2008, ApJ, 679, 655

Kalemci E., Dincer T., Tomsick J. A., Buxton M. M., Bailyn C. D., Chun Y. Y., 2013, ApJ, 779, 95

Kalemci E., Tomsick J. A., Buxton M. M., Rothschild R. E., Pottschmidt K., Corbel S., Brocksopp C., Kaaret P., 2005, ApJ, 622, 508

Kalemci E., Tomsick J. A., Rothschild R. E., Pottschmidt K., Corbel S., Kaaret P., 2006a, ApJ, 639, 340

Kalemci E., Tomsick J. A., Rothschild R. E., Pottschmidt K., Migliari S., Corbel S., Kaaret P., 2006b, in VI Microquasar Workshop: Microquasars and Beyond

Lewis F., Russell D. M., Fender R. P., Roche P., Clark J. S., 2008, in Microquasars and Beyond, p. 69

Maitra D., Markoff S., Brocksopp C., Noble M., Nowak M., Wilms J., 2009, MNRAS, 398, 1638

Makishima K., Maejima Y., Mitsuda K., Bradt H. V., Remillard R. A., Tuohy I. R., Hoshi R., Nakagawa M., 1986, ApJ, 308, 635

Malzac J. et al., 2006, A&A, 448, 1125

Markoff S., Falcke H., Fender R., 2001, A&A, 372, L25

Markoff S., Nowak M. A., Wilms J., 2005, ApJ, 635, 1203

McClintock J. E., Remillard R. A., 2006, Black hole binaries, Lewin, W. H. G. & van der Klis, M., ed., pp. 157–213

McConnell M. L. et al., 2000, ApJ, 543, 928

Miller-Jones J. C. A., Sivakoff G. R., 2012, The Astronomer's Telegram, 4394

Miyakawa T., Yamaoka K., Homan J., Saito K., Dotani T., Yoshida A., Inoue H., 2008, PASJ, 60, 637

Motta S., Belloni T., Homan J., 2009, MNRAS, 400, 1603

Muñoz-Darias T. et al., 2013, MNRAS, 432, 1133

Nowak M. A. et al., 2011, ApJ, 728, 13

Pe'er A., Markoff S., 2012, ApJ, 753, 177

Poutanen J., Svensson R., 1996, ApJ, 470, 249

Poutanen J., Veledina A., 2013, Space Sci.Rev., arxiv/1312.2761

Rau A., Knust F., Kann D. A., Greiner J., 2012, The Astronomer's Telegram, 4380

Reynolds M. T., Miller J. M., 2013, ApJ, 769, 16

Russell D. M. et al., 2012, MNRAS, 419, 1740

Russell D. M., Lewis F., Munoz-Darias T., Kalemci E., 2013a, The Astronomer's Telegram, 5084

Russell D. M., Maitra D., Dunn R. J. H., Markoff S., 2010, MNRAS, 405, 1759

Russell D. M., Miller-Jones J. C. A., Maccarone T. J., Yang Y. J., Fender R. P., Lewis F., 2011, ApJ, 739, L19

Russell D. M. et al., 2013b, ApJ, 768, L35

Russell T. D., Soria R., Miller-Jones J. C. A., Curran P. A., Markoff S., Russell D. M., Sivakoff G. R., 2014, MNRAS, 439, 1390

Sbarufatti B. et al., 2012, The Astronomer's Telegram, 4383

Sbarufatti B., Kennea J. A., Stroh M. C., Burrows D. N., Evans P. A., Beardmore A. P., Krimm H. A., Gehrels N., 2013, The Astronomer's Telegram, 4782

Soleri P. et al., 2013, MNRAS, 429, 1244

Tomsick J. A., Del Santo M., Belloni T., 2012, The Astronomer's Telegram, 4393

Veledina A., Poutanen J., Vurm I., 2013, MNRAS, 430, 3196

Verner D. A., Ferland G. J., Korista K. T., Yakovlev D. G., 1996, ApJ, 465, 487

Vovk I. et al., 2012, The Astronomer's Telegram, 4381

Wilms J., Allen A., McCray R., 2000, ApJ, 542, 914

Zurita C. et al., 2002, MNRAS, 334, 999